Facile synthesis of CoOOH@MXene to Activate Peroxymonosulfate for Efficient Degradation of Sulfamethoxazole: Performance and Mechanism Investigation

Xinjing Xia
Hunan University
Lin Deng (lindeng@hnu.edu.cn)
Hunan University
Lingfang Yang
Hunan University
Zhou Shi
Hunan University

Research Article

Keywords: MXene, CoOOH, Peroxymonosulfate activation, Sulfamethoxazole degradation, Mechanism analysis

Posted Date: January 19th, 2022

DOI: https://doi.org/10.21203/rs.3.rs-1101655/v1

Version of Record: A version of this preprint was published at Environmental Science and Pollution Research on March 11th, 2022. See the published version at https://doi.org/10.1007/s11356-022-19664-3.

Abstract

Using MXene as substrate, CoOOH@MXene with different mass content of CoOOH were prepared and used to active PMS for the sulfamethoxazole (SMX) degradation. The samples characterizations demonstrated the successful preparation of CoOOH@MXene. CoOOH@MXene possessed much higher BET surface area (183.82 m^2/g) than CoOOH (85.36 m^2/g) and MXene (6.89 m^2/g) due to the good dispersibility of CoOOH particles on MXene. Due to its large surface area, 1.3CoOOH@MXene displayed the best catalytic performance for the degradation of SMX. With 0.2 g/L of 1.3CoOOH@MXene and 0.5 mM of PMS, 20 μM of SMX was completely eliminated in 10 min. The degradation followed pseudo-first-order kinetic model well, with rate constants of 0.33 min^{-1} and 0.054 min^{-1} for 1.3CoOOH@MXene and CoOOH. Influencing factors of initial pH, catalyst dosage, PMS concentration, SMX concentration and co-existing anions on SMX degradation were assessed systematically. Recycling tests verified the excellent reusability and stability of the catalyst. Quenching experiments and electron paramagnetic resonance analysis substantiated that $^1O_2$ played a leading role. Moreover, the intermediates were identified, and degradation pathways and activation mechanism of CoOOH@MXene for PMS were proposed. This work may highlight the application of MXene with transition metals in PMS activation.

1. Introduction

Antibiotics are continually detected in the water environments. Due to their high toxicity and possibility of producing resistant bacteria, they pose a huge threat to aquatic organisms and human health (Karkman et al. 2018). As a universally used sulfonamide antibiotics, sulfamethoxazole (SMX) presents in both the wastewater discharged from pharmaceutical manufacturing factories and conventional wastewater treatment plants (Liu et al. 2012). Unfortunately, due to the chemical stability and poor biodegradability of SMX, the traditional wastewater treatment techniques are unable to thoroughly eliminate SMX from aqueous solution (Müller et al. 2013). Hence, there is an urgent need to develop an effective technology to exhaustively remove SMX to minimize its perniciousness.

Advanced oxidation processes (AOPs) have increasingly drawn widespread attention and exhibits great development prospects as this approach can produce powerful reactive species to oxidize stubborn macromolecular organic contaminants into innocuous small compounds (Zhou et al. 2018). $SO_4^{\bullet-}$ based AOPs have stronger oxidation ability, higher selectivity, wider pH adaptation range, and have showed fascinating performance in water and wastewater treatment (Duan et al. 2019, Zhang et al. 2020a). Generally, $SO_4^{\bullet-}$ can be obtained through activating peroxymonosulfate (PMS) or persulfate (PS) by heat (Yang et al. 2010), ultraviolet (UV) (Rehman et al. 2018), alkaline and transition metals (Du et al. 2016, Yu et al. 2019). Without the requirements of external energy supply or chemical reagent consumption, transition metals activation (Co^{2+}, Cu^{2+}, Fe^{2+}, Fe^{3+}, Mn^{2+}, and Ni^{2+}) has been regarded as one of the most effective and feasible approach (Anipsitakis &Dionysiou 2004). Yet, the activation of transition metals in a homogeneous system is limited on account of the metal ions loss, discommodious recovery and inevitable sludge generation (Liang et al. 2012). Heterogeneous systems can overcome these

shortcomings. Accordingly, much efforts have been made to construct solid catalysts of transition metals especially Co based compounds (Zeng et al. 2017).

As a newly reported two-dimensional (2D) layered material, MXene consists of carbonitrides and transition metal carbides (Naguib et al. 2011). Thanks to its well-defined layered structure, excellent metal conductivity, abundant Lewis acid sites and surface functional groups, and structural stability (Anasori et al. 2017), MXene has been extensively applied in reinforcement for nanocomposites (Ling et al. 2014), water purification (Guo et al. 2015) and catalysis (Zhao et al. 2017). Besides, a great deal of hydroxyl, carboxyl and epoxy groups on MXene are supposed to provide superior water dispersibility and powerful anchoring effect for free cations as well (Peng et al. 2014). These merits promote the production and uniform distribution of transition metal nanoparticles. As a result, MXene is considered to be a promising supporting material for nanocatalysts.

Liu et al. reported that Co_3O_4@MXene achieved higher rate constant BPA degaradation (0.3984 min^{-1}) than Co_3O_4 (0.1439 min^{-1}) (Liu et al. 2018). Wang et al. presented that the rhombus Co(OH)F@MXenes exhibited much higher catalytic activity and stability than Co_3O_4 and CoO (Wang et al. 2020). Ding et al. demonstrated that MXene could promote the dispersion of Fe_2O_3 nanoparticles, thereby improving the catalytic performance (Ding et al. 2020). Our group firstly demonstrated that Lewis-acid sites on MXene was crucial in PMS activation over Prussian blue analogues@MXene (Zeng et al. 2021). Overall, previous literature suggested that the employment of MXene as a support material could remarkably enhance the catalytic activity, showing good prospects in organics degradation.

As a naturally occurring mineral, cobalt oxyhydroxide (CoOOH) has received increasingly interests as an alternative catalyst to activate PMS owing to its effective electron transfer rate, high hydrophilicity with plentiful of hydroxyl groups and active sites (Decree et al. 2015). Besides, the resulting $CoOH^+$ is regarded as efficient active species and the limiting step of the overall catalytic reaction rate in Co^{2+} combined PMS system (Shi et al. 2014). Though promising, the catalytic activity of CoOOH nanoparticles for PMS is required to be enhanced. Herein, we synthesized a novel CoOOH@MXene by supporting CoOOH nanoparticles onto the multi-layered MXene via co-precipitation method. It's expected that MXene would greatly increase the dispersibility and catalytic activity of CoOOH nanoparticles. Nevertheless, to date, there is few study on examining the catalytic activity of CoOOH@MXene in AOPs. The obtained CoOOH@MXene was characterized and used to activate PMS for SMX degradation. The catalytic performance was systematically assessed from the perspective of initial pH, catalyst dosage, PMS concentration, SMX concentration and co-existing anions. The active species participated in the catalytic system were identified by radical scavenging experiments and EPR analysis. The activation mechanism and oxidation intermediates of SMX were clarified as well.

2. Materials And Methods

2.1. Chemicals

Ti_3AlC_2 (MAX) powder (purity ≥ 98%) was acquired from Forsman Co., Ltd. (Beijing, China). PMS was purchased from Aladdin Biochemical Technology Co., Ltd (Shanghai, China). Other reagents were obtained from Sinopharm Chemical Reagent Co., Ltd. (Shanghai, China). In this study, all chemicals are of analytical grade without purification, and ultrapure water was used throughout the experiments produced by a Millipore system (Bedford, USA).

2.2. Synthesis of CoOOH@MXene

The synthesis procedure of CoOOH@MXene is schematically illustrated in Fig. 1. MXene used in this study was prepared by hydrofluoric acid etching method from the pristine Ti_3AlC_2 (Lukatskaya et al. 2013). The CoOOH@MXene was prepared by a modified chemical precipitation method. 0.1 g of the as-synthesized MXene and different mass of $CoCl_2·6H_2O$ (0.05, 0.13, 0.21 g) were mixed in 25 mL of ultrapure water and sonicated for 15 min to obtain a homogeneous mixture. Subsequently, 0.1 M of NaOH solution was added dropwise into the above mixture until the pH reached 11.5. After keeping the resulting solution in water bath (60 ℃) for 2 h, 5 mL H_2O_2 was injected into the solution and continued to react for 2 h. Finally, the resultant solids were washed and dried at 60 ℃. The products were named as *x*CoOOH@MXene, where *x* represented 0.5, 1.3, and 2.1 according to the designed weight ratio of MXene to $CoCl_2·6H_2O$.

Details on the characterization and experimental methods are described in Text S1-S2.

3. Results And Discussion

3.1. Characterization

The microstructure and morphology of MXene and 1.3CoOOH@MXene were analyzed using SEM. From Fig. 2a, it can be clearly seen that the dense layer structure of Ti_3AlC_2 transforms into accordion-like MXenes after being etched in HF solution. As depicted in Fig. 2b and c, the as-synthesized 1.3CoOOH@MXene still maintains the layered structure of MXene and many tiny particles are obviously loaded onto the surface and interlayers of MXene, which is probably a connection with the loading of CoOOH nanoparticles. The SEM images imply that the surface of 1.3CoOOH@MXene is much rougher than the pure MXene. Meanwhile, EDS was also recorded to reveal the chemical composition. As seen in Fig. 2d, there are four different elements (Ti, C, O and Co) on the surface of the 1.3CoOOH@MXene composites, and all elements were well distributed in the whole area.

The crystal information of MXene and 1.3CoOOH@MXene were identified by XRD patterns (Fig. 2e). Clearly, the characteristic diffraction peaks located at 20.2°, 36.9°, 38.8°, 46.2°, 50.6°, 62.4°, 65.3° and 69.2° corresponds to the (003), (101), (012), (104), (015), (017), (110) and (113) planes of CoOOH (JCPDS No. 73-1213), respectively (Lyu et al. 2019). The diffraction signals appearing at 8.9°, 18.4°, 36.0°, 41.9° and 59.5° can be ascribed to the (002), (004), (103), (105) and (110) plane corresponding to the MXene crystal (Zhang et al. 2018). For the XRD patterns of the composite, the characteristic peaks of (004),

(103) and (110) belonging to MXene can be distinguished, but the intensity is significantly weakened, confirming that the crystal structure of MXene is well maintained. The disappeared (002) peak is probably ascribed to the loss of titanium from MXene. Further, the characteristic peaks of CoOOH is obviously strengthened with increasing the mass ratio of CoOOH. The above observation indicates the successful synthesis of CoOOH@MXene composites.

FTIR spectra was then performed to investigate the difference of functional groups on CoOOH, MXene and 1.3CoOOH@MXene. From Fig. 2f, for the CoOOH, three distinguishable peaks at 581.5, 1839, and 3430 cm^{-1} are associated with the Co-O double bond, Co-OH group and H-bonded hydroxyl group (-OH), respectively (Li et al. 2015a). As for the MXene, the peak at 1059 cm^{-1} can be assigned to the C-F bond, and the peak at 1172 cm^{-1} represents the C-O group. The peaks at 1631 and 3446 cm^{-1} belong to the bending vibration of -OH and the asymmetric stretching of -OH, respectively (Xiu et al. 2018). For the 1.3CoOOH@MXene nanocomposite, the primary characteristic peaks of the original CoOOH and MXene are all observed, and no additional functional groups are detected. This further reveals the successful construction of CoOOH@MXene.

The BET surface area of CoOOH, MXene and various CoOOH@MXene composites were determined by measuring the N_2 adsorption-desorption isotherms, and the results are illustrated in Fig. 2g and Table 1. All samples possess a typical type-IV isotherm with a hysteresis loop, evidencing the presence of mesopores. Specifically, MXene shows the BET surface area of 6.89 m^2/g, with a pore volume of 0.012 cm^3/g. The incorporation of CoOOH greatly increased the BET surface area, 160.99, 183.32, and 143.13 m^2/g for 0.5CoOOH@MXene, 1.3CoOOH@MXene, and 2.1CoOOH@MXene, respectively, with corresponding pore volumes of 0.11, 0.24, and 0.23 cm^3/g, respectively. The higher BET surface area of the composite was probably due to the good dispersibility of CoOOH particles on the MXene substrate. A higher BET surface area can supply sufficient active sites, thereby achieving higher catalytic activity (Chen et al. 2019). This is consistent with the results of degradation experiments in the following part.

Table 1. BET surface area and pore properties of catalysts.

Samples	BET surface area (m^2/g)	Total pore volume (m^3/g)
MXene	6.89	0.012
CoOOH	85.36	0.37
0.5CoOOH@MXene	160.99	0.11
1.3CoOOH@MXene	183.32	0.24
2.1CoOOH@MXene	143.13	0.23

3.2. Performance of CoOOH@MXene for SMX degradation

The catalytic performance of CoOOH@MXene was investigated by the effect of catalyst activation of PMS to remove SMX. Fig. 3a shows the removal capacity of SMX in different reaction systems. PMS was

ineffective for SMX degradation because of its low tendency towards producing enough active radicals. The MXene also could not activate PMS effectively. And the 1.3CoOOH@MXene could hardly remove SMX either due to the terrible adsorption capacity. By contrast, with the occurrence of PMS and CoOOH@MXene composites, an abrupt drop of SMX concentration occurred, demonstrating that the CoOOH@MXene was efficient activator for PMS, that benefiting the SMX degradation. From the figure, the removal rate reached 99% in the 1.3CoOOH@MXene activated PMS system within 10 min.

The degradation process is matched well with the pseudo-first-order kinetics, which can be expressed through the following correlation equation: $-\ln(C/C_0) = k_{obs}t$, where C_0 represents the initial SMX concentration, C represents the SMX concentration at a certain moment during the reaction, and k_{obs} represents the apparent kinetic rate constant of SMX degradation (min^{-1}). As shown in Fig. 3b, CoOOH has the lowest k_{obs} value (0.054 min^{-1}), while k_{obs} achieved by 0.5CoOOH@MXene, 1.3CoOOH@MXene and 2.1CoOOH@MXene are 0.175, 0.334 and 0.211 min^{-1}, respectively. The excellent catalytic activity of the composites was attributed to that MXene inhibited the agglomeration of small size of CoOOH. It was noted that 1.3CoOOH@MXene possessed the highest BET surface area, which contributed to PMS activation for SMX degradation as well. Yet, excessive CoOOH loading resulted in an observable declined degradation efficiency, which was probably caused by the overlapping of active sites (Shi et al. 2014). Because of the highest catalytic activity, 1.3CoOOH@MXene was utilized for the follow-up experiments.

3.3. Effects of operating parameters on catalytic activity

So as to further examine the catalytic activity of 1.3CoOOH@MXene, the effects of initial pH, catalyst dosage, PMS concentration, SMX concentration and co-existing inorganic anions on the SMX degradation by the catalytic system was studied. At first, experiments on the SMX degradation were performed at pH=3.0-9.0 as shown in Fig. 3c. With the solution pH increased from 3.0 to 9.0, the removal efficiency gradually enhanced. Compared with the acidic condition, the alkaline condition seemed to be more conducive to the SMX removal. At pH of 9.0, SMX could be absolutely eliminated in less than 5 min, while the degradation was only 71.4% when the initial pH was set at 3.0. The obtained k_{obs} values for pH of 3.0, 5.0, 7.0 and 9.0 were found to be 0.28, 0.35, 0.43 and 0.71 min^{-1}, respectively (the inset in Fig. 3c).

In general, the SMX removal at different pH was influenced by the pK_a of PMS (9.4), the point of zero charge (pH_{PZC}) of 1.3CoOOH@MXene and the pK_a of SMX (pK_{a1} = 1.6, pK_{a2} = 5.7) (Zhang et al. 2020c). Firstly, with increasing solution pH to 9.0, the amount of SO_5^{2-} in the system would sharply increase. SO_5^{2-} is easier to be activated to produce $SO_4^{\bullet-}$ than HSO_5^- (Hong et al. 2020). On the other hand, as displayed in Fig. S1, the pH_{PZC} of 1.3CoOOH@MXene was 4.7. That's to say, at pH below 4.7, the surface charge of the catalyst was positive, while at pH value higher than 4.7, the catalyst surface would be negatively charged. Under acidic pH, plenty of hydrogen bonds were produced between H^+ and O–O groups of HSO_5^-, preventing the contact between PMS and the positively charged surface of 1.3CoOOH@MXene. This resulted in a lower removal of SMX (Yan et al. 2019). Besides, the excess H^+ in the solution would consume the generated free radicals as well. With regard to alkaline conditions, OH^-

participated in the activation process of PMS, thereby accelerating the formation of active species (Chen et al. 2020). Finally, the solution pH also has a considerable influence on the existing species of SMX. At pH below 5.7, SMX exists primarily in non-protonated form. Once the pH surpasses 5.7, SMX exists in a deprotonated form. As reported, the reactivity of the deprotonated SMX was higher than the non-protonated SMX (Wang &Wang 2018), and this was helpful for the degradation.

Figure S2a exhibits the SMX degradation at various catalyst dosages (0.1, 0.2, 0.3 and 0.4 g/L). At a fixed PMS concentration (0.5 mM), in 5 min, the degradation rate increased from 59.8–99.4% as the catalyst dose improved from 0.1 to 0.4 g/L. A higher catalyst dose could definitely supply more active centers for PMS activation, thereby enhancing the PMS utilization rate. The influence of PMS concentration on the SMX removal is depicted in Fig. S2b. The degradation enhanced gradually with the improvement of PMS concentration at a fixed catalyst dosage. At PMS concentration of 0.3 mM, the degradation rate reached 95.4% in 10 min; when the PMS concentration was 0.9 mM, it only took less than 5 min to achieve a nearly complete elimination of SMX. Higher PMS concentration corresponds to a faster degradation owing to more number of active species produced by PMS. In view of the economic aspect, 0.2 g/L of 1.3CoOOH@MXene and 0.5 mM of PMS were chosen in the following tests. Fig. S2c represents initial SMX concentration (10, 20, 30 and 40 μM) on the performance of 1.3CoOOH@MXene in the catalytic system. As the pollutant concentration increased from 10 to 40 μM, the degradation rate was restrained step by step. This may be attributed to the insufficient amount of oxidizing species (Li et al. 2017).

Cl^-, F^-, HCO_3^- and $H_2PO_4^-$ are frequently detected in water bodies. Thus, the effect of coexisting inorganic ions on the SMX removal was studied as well. Fig. S3 represents the influences of Cl^-, F^-, HCO_3^- and $H_2PO_4^-$ (5, 10 and 30 mM) on SMX removal. Obviously, adding Cl^- or F^- ions greatly accelerated the degradation of SMX. When the concentration of Cl^- was 0, 5, 10 and 30 mM, the removal rates within 1 min were found to be 32.2%, 62.5%, 76.1% and 84.8%, respectively. This result was mainly related to that Cl^- could react with PMS to generate hypochlorite acid (HOCl) (Eqs. (1)–(2)), which accelerated the SMX degradation (Ao &Liu 2017, Deng et al. 2013).

$$Cl^- + HSO_5^- \rightarrow SO_4^{2-} + HOCl \quad (1)$$

$$2Cl^- + HSO_5^- + H^+ \rightarrow SO_4^{2-} + Cl_2 + H_2O \quad (2)$$

Similarly, as the concentration of F^- improved from 0 to 30 mM, the degradation rate in 1 min enhanced significantly from 32.1–97.4%. Nevertheless, the TBA quenching tests in the following paragraphs showed that the system lacked $^{\bullet}OH$ radicals. Hence, $^{\bullet}OH$ may be produced on the surface of the catalyst. F^- could release free radicals on the catalyst surface into the solution, thereby promoting the degradation of SMX (Zeng et al. 2020). Fig. S3c shows that the existence of HCO_3^- decreased the SMX degradation. Bicarbonate can react with $^{\bullet}OH$ and $SO_4^{\bullet-}$ to bicarbonate radicals ($CO_3^{\bullet-}$) (Eqs. (3), (4)), which has low reactivity with SMX (Sharma et al. 2015).

$SO_4^{\bullet-} + HCO_3^- \rightarrow SO_4^{2-} + CO_3^{\bullet-} + H^+$ (3)

$^{\bullet}OH + HCO_3^- \rightarrow CO_3^{\bullet-} + H_2O$ (4)

As for $H_2PO_4^-$, it showed a imperceptible influence on the SMX degradation in the 1.3CoOOH@MXene activated PMS system (Fig. S3d).

3.4. Stability and reusability test

Stability and reusability of catalysts are essential for practical application in view of the economic aspect. In order to study the structure stability of 1.3CoOOH@MXene, Co ions dissolution concentration under different pH values was assessed. From Fig. S4a, the Co ion dissolution concentration at pH 9.0 was 14.8 μg/L, and it increased gradually with the decrease of pH. Yet, the leaching Co ions concentration was much lower than the legal limit of 1.0 mg/L (GB 8978-2002) stipulated by the China Environmental Protection Agency. This indicated the impressive stability of the as-prepared 1.3CoOOH@MXene.

Repeating tests were carried out to assess the reusability of 1.3CoOOH@MXene as well. At the end of each cycle, the catalyst was collected by centrifugation, washed with large amount of ethanol and ultrapure water, and then dried at 60℃. As illustrated in Fig. 3d, there was no significant degradation loss during the consecutive runs. In the fourth run, the removal rate was even higher than 90%, demonstrating the superior recyclability of 1.3CoOOH@MXene. In addition, the recovered catalyst were also characterized by XRD patterns (Fig. S4b). No significant difference was detected between the fresh and used catalyst, proving its excellent physicochemical stability.

3.5. Mechanisms of PMS activation over CoOOH@MXene

3.5.1 Radical identification

To recognize reactive oxygen species (ROS) involved in the system of 1.3CoOOH@MXene/PMS, a series of quenching experiments were performed. In general, methanol (MeOH) can capture both $^{\bullet}OH$ and $SO_4^{\bullet-}$, whereas *tert*-butyl alcohol (TBA) is used as a quencher of $^{\bullet}OH$ (Miao et al. 2018). *p*-benzoquinone (BQ) is applied to scavenge $O_2^{\bullet-}$ (Zhang et al. 2020b), and furfuryl alcohol (FFA) has a high reaction rate constant for $^1O_2$ (Li et al. 2019). As shown in Fig. 4a, almost no inhibition role of TBA in the SMX removal was observed even if its concentration was 500 times as that of PMS. On the contrast, the addition of 250 mM MeOH greatly declined the degradation rate to 40%, indicating that $SO_4^{\bullet-}$ was mainly involved in SMX oxidation reaction. However, excess MeOH (250 mM) could not completely inhibit the degradation, implying the involvement of some other ROS. Both BQ and FFA showed severe suppression on the oxidation process, especially when the FFA concentration was 10 mM the degradation was significantly inhibited to 10.7%. The above phenomenon suggested that $^1O_2$ played the vital role for SMX degradation, while $O_2^{\bullet-}$ and $SO_4^{\bullet-}$ took the second place, while $^{\bullet}OH$ just provided limited activity.

To valid the involved ROS intuitively, the electron paramagnetic resonance (EPR) spectroscopy was carried out with spin-trapping agents of 5-dimethyl-pyrroline-N-oxide (DMPO) or 2,2,6,6-tetramethyl-4-piperidine (TEMP). From Fig. 4b, no conspicuous signals was found in the presence of PMS alone. Whereas strong representative 1:2:1:2:1:2:1 heptet signals was observed, which was assigned to the combined signals of DMPO-OH and DMPO-SO_4 adducts. This further evidenced the existence of $^{\bullet}OH$ and $SO_4^{\bullet-}$. Simultaneously, the EPR spectra corroborated the inference that $O_2^{\bullet-}$ was produced on the basis of the characteristic peaks in Fig. 4c. Additionally, a 1:1:1 triplet signal related to TEMP-$^1O_2$ could also be detected (Fig. 4c) (Wang et al. 2016). According to the above analyses, $^{\bullet}OH$, $SO_4^{\bullet-}$, $O_2^{\bullet-}$ and $^1O_2$ all participated in the oxidative degradation of SMX, and $^1O_2$ played a leading role.

3.5.2 Activation mechanisms analysis

To better understand the catalytic mechanism of the as-synthesized CoOOH@MXene composites in PMS activation, the valance states and species transformation of Co and O before and after the oxidation reaction were further analyzed through X-ray photoelectron spectroscopy (XPS). The full-scale XPS spectra of 1.3CoOOH@MXene shown in Fig. 5a illustrates the main element of Co, O, Ti, and C. Fig. 5b depicts the high-resolution XPS spectrum of Co 2p. Two peaks at 781.5 and 796.5 eV corresponds to Co $2p_{3/2}$ and Co $2p_{1/2}$, respectively (Gong et al. 2017). In the deconvoluted spectrum, the peak of Co $2p_{3/2}$ at 781.6 eV and Co $2p_{1/2}$ at 797.3 eV corresponded to Co(III), and the peak of Co $2p_{3/2}$ at 783.5 eV and Co $2p_{1/2}$ at 798.5 eV signified Co(II) (Wu et al. 2020). Meanwhile, the peaks spotted at 787.5 and 802.5 eV were attributed to satellite peaks of Co $2p_{3/2}$ and Co $2p_{1/2}$ spin-orbits (Li et al. 2014). The overall Co intensity of 62% and 38% were assigned to Co(III) and Co(II) on the fresh 1.3CoOOH@MXene, while the relative proportion of Co(III) declined to 57% and Co(II) increased to 43% on the used one. The increased proportion of Co(II) was attributed to the reduction of Co(III) to Co(II), which demonstrated the participation of the redox pairs of Co(III)−Co(II)−Co(III) in the SMX degradation in the catalytic system. The XPS spectra of O 1s could be resolved into three individual peaks, 532.9, 531.3, and 529.9 eV representing the molecular water adsorbed on the surface (O_{ads}), metal hydroxide (Co–OH) and metal oxide (Co–O), respectively (Zhu et al. 2018). After the catalytic reaction, the O_{ads} amount dropped from 43–31%, indicating the participation of H_2O. Surprisingly, the relative proportion of Co–OH sharply grew from 28–42% because of the formation of $CoOH^+$, which was the most effective oxygen species to activate PMS and played a crucial role in the activation process (Song et al. 2018).

On the basis of the above discussion, a tentative catalytic mechanism for PMS activation by 1.3CoOOH@MXene was unveiled (Fig. 6). At first, PMS attached on the catalyst surface reacted with Co(III) to produce $SO_5^{\bullet-}$ and Co(II) via Eq. (5) (Ghanbari &Moradi 2017). In the meantime, the reaction between Co(II) and HSO_5^- resulted in the formation of $^{\bullet}OH$ and $SO_4^{\bullet-}$ (Eqs. (6), (7)) (Chen et al. 2017). Meanwhile, Co(II) could react with adsorbed H_2O molecules to form $CoOH^+$ complexes on the catalyst surface, and $CoOH^+$ contributed to the generation of $SO_4^{\bullet-}$ as well (Eqs. (8), (9)) (Tan et al. 2017). After PMS decomposition (Eqs. (10)), the formed SO_5^{2-} would react with H_2O to yield H_2O_2 (Eqs. (11)).

Subsequently, H_2O_2 would rapidly react with $^{\bullet}OH$ to develop $HO_2^{\bullet-}$ (Eqs. (12)), and then $O_2^{\bullet-}$ could be further released (Eqs. (13)) (Qi et al. 2016). $^1O_2$ in this study was evoked by the recombination of $O_2^{\bullet-}$ in the system according to Eq. (14) (Li et al. 2015b). On the other hand, $^1O_2$ could be slowly generated through Eq. (15) (Ball &Edwards 1956). Continuously, the formed active species ($^1O_2$, $^{\bullet}OH$, $SO_4^{\bullet-}$, and $O_2^{\bullet-}$) oxidized SMX into intermediates and might even mineralize them into CO_2 and H_2O (Eq. (16)).

$Co(III) + HSO_5^- \rightarrow Co(II) + SO_5^{\bullet-} + H^+$ (5)

$Co(II) + HSO_5^- \rightarrow Co(III) + SO_4^{\bullet-} + OH^-$ (6)

$Co(II) + HSO_5^- \rightarrow Co(III) + SO_4^{2-} + {}^{\bullet}OH$ (7)

$Co(II) + H_2O \rightarrow CoOH^+ + H^+$ (8)

$CoOH^+ + HSO_5^- \rightarrow CoO^+ + SO_4^{\bullet-} + H_2O$ (9)

$HSO_5^- \rightarrow H^+ + SO_5^{2-}$ (10)

$SO_5^{2-} + H_2O \rightarrow SO_4^{2-} + H_2O_2$ (11)

$H_2O_2 + {}^{\bullet}OH \rightarrow HO_2^{\bullet-} + H_2O$ (12)

$HO_2^{\bullet-} \rightarrow H^+ + O_2^{\bullet-}$ (13)

$2O_2^{\bullet-} + 2H_2O \rightarrow {}^1O_2 + H_2O_2 + 2OH^-$ (14)

$HSO_5^- + SO_5^- \rightarrow HSO_4^- + SO_4^{2-} + {}^1O_2$ (15)

$^1O_2$ / $^{\bullet}OH$ / $SO_4^{\bullet-}$ / $O_2^{\bullet-}$ + SMX → degradation intermediates → $CO_2 + H_2O$ (16)

3.6. Possible degradation pathways and toxicity evaluation of intermediates

To clarify the degradation process of SMX in the 1.3CoOOH@MXene activated PMS system, LC-MS was employed to recognize degradation intermediates. The MS spectra are shown in Fig. S5, and ten possible intermediates obtained are listed in Table S1. According to the identified intermediates and previous reports, four feasible degradation pathways were put forward in Fig. 7. In route 1, the amine group on the benzene ring in SMX was oxidized to form nitroso-SMX (P3) (Du et al. 2018). Then, P3 was then oxidized to generate P7 and P10 via deep hydroxylation and cleavage of unsaturated bonds, followed by the production of P8 and P9 (Liu et al. 2017). In route 2, the S—N bond was attacked by reactive oxygen species to yield P5 and P10 (Lai et al. 2018). In route 3, the opening of isoxazole ring occurred, leading to the generation of P4. Then, the C—N bond of P4 was cleaved by an electron-transfer reaction to produce

P5 and P6 (Bao et al. 2019). In route 4, the hydroxylation of heterocyclic ring occurred to induce P2. The methyl group on heterocycle of isoxazole was further oxidized to P1 due to the attack of $SO_4^{\bullet-}$ and $^{\bullet}OH$ (Mohatt et al. 2011).

Furthermore, the ecological structure activity relationship (ECOSAR) program was applied to predict the biotoxicity of SMX and its oxidation intermediates. From Fig. S6 and Table S2, the LC_{50} value of SMX toward fish and daphnia are calculated as 410.762 and 1.872 mg/L, and the EC_{50} value of SMX toward green algae is 6.615 mg/L. The corresponding ChVs for fish, daphnia and green algae are 2.337, 0.086, and 10.402 mg/L, respectively. Thus, SMX can be categorized as a extremely toxic organic pollutant (Chen et al. 2020). After the oxidation process, the acute and chronic toxicities of all intermediates to three typical aquatic organisms are less than that of SMX (except the LC50 values of P3, P5 and P10). This reveals that activating PMS by CoOOH@MXene to degrade SMX is of great significance to the safety of water environment.

4. Conclusions

Novel CoOOH@MXene with different mass ratio of CoOOH were successfully prepared and applied to activate PMS for the SMX degradation. The CoOOH@MXene displayed impressive catalytic activity. The catalytic performance followed the order: 1.3CoOOH@MXene (0.33 min^{-1}) > 2.1CoOOH@MXene (0.21 min^{-1}) > 0.5CoOOH@MXene (0.18 min^{-1}) > CoOOH (0.054 min^{-1}), which was dependent on their specific surface area. Increasing initial solution pH promoted the SMX degradation, with corresponding rate constants of 0.28, 0.35, 0.43, and 0.71 min^{-1} for pH of 3, 5, 7, and 9, respectively. Increasing PMS concentration and 1.3CoOOH@MXene dose improved the degradation as well. The addition of Cl^- and F^- greatly accelerated the degradation rate of SMX, while the presence of HCO_3^- lowered the degradation. Moreover, the as-synthesized showed excellent recyclability and stability in the consecutive runs with low cobalt ions leaching. Four degradation pathways were proposed according to the recognized degradation intermediates. According to the quenching tests and EPR analysis, $^{\bullet}OH$, $SO_4^{\bullet-}$, $O_2^{\bullet-}$ and $^1O_2$ radicals all participated in the SMX degradation, and $^1O_2$ played a primary role. Overall, 1.3CoOOH@MXene could be a promising candidate for activating PMS for the SMX degradation.

Declarations

Author contribution

Xinjing Xia: methodology, formal analysis, data curation, and original draft writing; Lin Deng: Writing-review and editing, Funding acquisition, resources, and supervision; Lingfang Yang: intermediate identification and mechanism analysis; Zhou Shi: Writing-review and editing and funding acquisition.

Funding

This work was financially supported by the Natural Science Foundation of Hunan Province (2021JJ40069) and National Natural Science Foundation of China (51878256).

Availability of data and materials

The datasets used and/or analyzed during the current study are available from the corresponding author on reasonable request.

Ethics approval and consent to participate The local Ethics Committee of Hunan University approved the consent form.

Consent for publication Not applicable.

Competing interests The authors declare no competing interests.

References

Anasori B, Lukatskaya MR, Gogotsi Y (2017): 2D metal carbides and nitrides (MXenes) for energy storage. Nature Reviews Materials 2, 1-17

Anipsitakis GP, Dionysiou DD (2004): Radical generation by the interaction of transition metals with common oxidants. Environmental science & technology 38, 3705-3712

Ao X, Liu W (2017): Degradation of sulfamethoxazole by medium pressure UV and oxidants: peroxymonosulfate, persulfate, and hydrogen peroxide. Chemical Engineering Journal 313, 629-637

Ball DL, Edwards JO (1956): The kinetics and mechanism of the decomposition of Caro's acid. I. Journal of the American Chemical Society 78, 1125-1129

Bao Y, Oh W-D, Lim T-T, Wang R, Webster RD, Hu X (2019): Elucidation of stoichiometric efficiency, radical generation and transformation pathway during catalytic oxidation of sulfamethoxazole via peroxymonosulfate activation. Water research 151, 64-74

Chen F, Huang G-X, Yao F-B, Yang Q, Zheng Y-M, Zhao Q-B, Yu H-Q (2020): Catalytic degradation of ciprofloxacin by a visible-light-assisted peroxymonosulfate activation system: performance and mechanism. Water research 173, 115559

Chen L, Cai T, Sun W, Zuo X, Ding D (2017): Mesoporous bouquet-like Co3O4 nanostructure for the effective heterogeneous activation of peroxymonosulfate. Journal of the Taiwan Institute of Chemical Engineers 80, 720-727

Chen L, Jia J, Ran R, Song X (2019): Nickel doping MnO2 with abundant surface pits as highly efficient catalysts for propane deep oxidation. Chemical Engineering Journal 369, 1129-1137

Decree S, Pourret O, Baele J-M (2015): Rare earth element fractionation in heterogenite (CoOOH): implication for cobalt oxidized ore in the Katanga Copperbelt (Democratic Republic of Congo). Journal of Geochemical Exploration 159, 290-301

Deng J, Shao Y, Gao N, Xia S, Tan C, Zhou S, Hu X (2013): Degradation of the antiepileptic drug carbamazepine upon different UV-based advanced oxidation processes in water. Chemical Engineering Journal 222, 150-158

Ding M, Chen W, Xu H, Shen Z, Lin T, Hu K, hui Lu C, Xie Z (2020): Novel α-Fe2O3/MXene nanocomposite as heterogeneous activator of peroxymonosulfate for the degradation of salicylic acid. Journal of hazardous materials 382, 121064

Du J, Bao J, Liu Y, Ling H, Zheng H, Kim SH, Dionysiou DD (2016): Efficient activation of peroxymonosulfate by magnetic Mn-MGO for degradation of bisphenol A. Journal of hazardous materials 320, 150-159

Du J, Guo W, Wang H, Yin R, Zheng H, Feng X, Che D, Ren N (2018): Hydroxyl radical dominated degradation of aquatic sulfamethoxazole by Fe0/bisulfite/O2: kinetics, mechanisms, and pathways. Water research 138, 323-332

Duan Z, Deng L, Shi Z, Zhang H, Zeng H, Crittenden J (2019): In situ growth of Ag-SnO2 quantum dots on silver phosphate for photocatalytic degradation of carbamazepine: Performance, mechanism and intermediates toxicity assessment. Journal of colloid and interface science 534, 270-278

Ghanbari F, Moradi M (2017): Application of peroxymonosulfate and its activation methods for degradation of environmental organic pollutants. Chemical Engineering Journal 310, 41-62

Gong C, Chen F, Yang Q, Luo K, Yao F, Wang S, Wang X, Wu J, Li X, Wang D (2017): Heterogeneous activation of peroxymonosulfate by Fe-Co layered doubled hydroxide for efficient catalytic degradation of Rhoadmine B. Chemical engineering journal 321, 222-232

Guo J, Peng Q, Fu H, Zou G, Zhang Q (2015): Heavy-metal adsorption behavior of two-dimensional alkalization-intercalated MXene by first-principles calculations. The Journal of Physical Chemistry C 119, 20923-20930

Hong Y, Zhou H, Xiong Z, Liu Y, Yao G, Lai B (2020): Heterogeneous activation of peroxymonosulfate by CoMgFe-LDO for degradation of carbamazepine: Efficiency, mechanism and degradation pathways. Chemical Engineering Journal 391, 123604

Karkman A, Do TT, Walsh F, Virta MP (2018): Antibiotic-resistance genes in waste water. Trends in microbiology 26, 220-228

Lai L, Yan J, Li J, Lai B (2018): Co/Al2O3-EPM as peroxymonosulfate activator for sulfamethoxazole removal: performance, biotoxicity, degradation pathways and mechanism. Chemical Engineering Journal

343, 676-688

Li C, Wu J, Peng W, Fang Z, Liu J (2019): Peroxymonosulfate activation for efficient sulfamethoxazole degradation by Fe3O4/β-FeOOH nanocomposites: Coexistence of radical and non-radical reactions. Chemical Engineering Journal 356, 904-914

Li J, Lu G, Wu G, Mao D, Guo Y, Wang Y, Guo Y (2014): Effect of TiO 2 crystal structure on the catalytic performance of Co 3 O 4/TiO 2 catalyst for low-temperature CO oxidation. Catalysis Science & Technology 4, 1268-1275

Li J, Ren Y, Ji F, Lai B (2017): Heterogeneous catalytic oxidation for the degradation of p-nitrophenol in aqueous solution by persulfate activated with CuFe2O4 magnetic nano-particles. Chemical Engineering Journal 324, 63-73

Li L, Wang C, Liu K, Wang Y, Liu K, Lin Y (2015a): Hexagonal cobalt oxyhydroxide–carbon dots hybridized surface: high sensitive fluorescence turn-on probe for monitoring of ascorbic acid in rat brain following brain ischemia. Analytical chemistry 87, 3404-3411

Li X, Liu J, Rykov AI, Han H, Jin C, Liu X, Wang J (2015b): Excellent photo-Fenton catalysts of Fe–Co Prussian blue analogues and their reaction mechanism study. Applied Catalysis B: Environmental 179, 196-205

Liang H, Sun H, Patel A, Shukla P, Zhu ZH, Wang S (2012): Excellent performance of mesoporous Co3O4/MnO2 nanoparticles in heterogeneous activation of peroxymonosulfate for phenol degradation in aqueous solutions. Applied Catalysis B: Environmental 127, 330-335

Ling Z, Ren CE, Zhao M-Q, Yang J, Giammarco JM, Qiu J, Barsoum MW, Gogotsi Y (2014): Flexible and conductive MXene films and nanocomposites with high capacitance. Proceedings of the National Academy of Sciences 111, 16676-16681

Liu G, Li X, Han B, Chen L, Zhu L, Campos LC (2017): Efficient degradation of sulfamethoxazole by the Fe (II)/HSO5− process enhanced by hydroxylamine: efficiency and mechanism. Journal of hazardous materials 322, 461-468

Liu X, Garoma T, Chen Z, Wang L, Wu Y (2012): SMX degradation by ozonation and UV radiation: a kinetic study. Chemosphere 87, 1134-1140

Liu Y, Luo R, Li Y, Qi J, Wang C, Li J, Sun X, Wang L (2018): Sandwich-like Co3O4/MXene composite with enhanced catalytic performance for Bisphenol A degradation. Chemical Engineering Journal 347, 731-740

Lukatskaya MR, Mashtalir O, Ren CE, Dall'Agnese Y, Rozier P, Taberna PL, Naguib M, Simon P, Barsoum MW, Gogotsi Y (2013): Cation intercalation and high volumetric capacitance of two-dimensional titanium carbide. Science 341, 1502-1505

Lyu C, He D, Chang Y, Zhang Q, Wen F, Wang X (2019): Cobalt oxyhydroxide as an efficient heterogeneous catalyst of peroxymonosulfate activation for oil-contaminated soil remediation. Science of The Total Environment 680, 61-69

Miao J, Sunarso J, Duan X, Zhou W, Wang S, Shao Z (2018): Nanostructured Co-Mn containing perovskites for degradation of pollutants: Insight into the activity and stability. Journal of hazardous materials 349, 177-185

Mohatt JL, Hu L, Finneran KT, Strathmann TJ (2011): Microbially mediated abiotic transformation of the antimicrobial agent sulfamethoxazole under iron-reducing soil conditions. Environmental science & technology 45, 4793-4801

Müller E, Schüssler W, Horn H, Lemmer H (2013): Aerobic biodegradation of the sulfonamide antibiotic sulfamethoxazole by activated sludge applied as co-substrate and sole carbon and nitrogen source. Chemosphere 92, 969-978

Naguib M, Kurtoglu M, Presser V, Lu J, Niu J, Heon M, Hultman L, Gogotsi Y, Barsoum MW (2011): Two-dimensional nanocrystals produced by exfoliation of Ti3AlC2. Advanced materials 23, 4248-4253

Peng Q, Guo J, Zhang Q, Xiang J, Liu B, Zhou A, Liu R, Tian Y (2014): Unique lead adsorption behavior of activated hydroxyl group in two-dimensional titanium carbide. Journal of the American Chemical Society 136, 4113-4116

Qi C, Liu X, Ma J, Lin C, Li X, Zhang H (2016): Activation of peroxymonosulfate by base: implications for the degradation of organic pollutants. Chemosphere 151, 280-288

Rehman F, Sayed M, Khan JA, Shah NS, Khan HM, Dionysiou DD (2018): Oxidative removal of brilliant green by UV/S2O82−, UV/HSO5−and UV/H2O2 processes in aqueous media: a comparative study. Journal of hazardous materials 357, 506-514

Sharma J, Mishra I, Dionysiou DD, Kumar V (2015): Oxidative removal of Bisphenol A by UV-C/peroxymonosulfate (PMS): kinetics, influence of co-existing chemicals and degradation pathway. Chemical Engineering Journal 276, 193-204

Shi P, Dai X, Zheng H, Li D, Yao W, Hu C (2014): Synergistic catalysis of Co3O4 and graphene oxide on Co3O4/GO catalysts for degradation of Orange II in water by advanced oxidation technology based on sulfate radicals. Chemical engineering journal 240, 264-270

Song F, Zhang H, Wang S, Liu L, Tan X, Liu S (2018): Atomic-level design of CoOH+−hydroxyapatite@ C catalysts for superfast degradation of organics via peroxymonosulfate activation. Chemical Communications 54, 4919-4922

Tan C, Gao N, Fu D, Deng J, Deng L (2017): Efficient degradation of paracetamol with nanoscaled magnetic CoFe2O4 and MnFe2O4 as a heterogeneous catalyst of peroxymonosulfate. Separation and

Purification Technology 175, 47-57

Wang F, Lai Y, Fang Q, Li Z, Ou P, Wu P, Duan Y, Chen Z, Li S, Zhang Y (2020): Facile fabricate of novel Co (OH) F@ MXenes catalysts and their catalytic activity on bisphenol A by peroxymonosulfate activation: The reaction kinetics and mechanism. Applied Catalysis B: Environmental 262, 118099

Wang J, Wang S (2018): Activation of persulfate (PS) and peroxymonosulfate (PMS) and application for the degradation of emerging contaminants. Chemical Engineering Journal 334, 1502-1517

Wang Y, Xie Y, Sun H, Xiao J, Cao H, Wang S (2016): Efficient catalytic ozonation over reduced graphene oxide for p-hydroxylbenzoic acid (PHBA) destruction: active site and mechanism. ACS applied materials & interfaces 8, 9710-9720

Wu X, Zhao W, Huang Y, Zhang G (2020): A mechanistic study of amorphous CoSx cages as advanced oxidation catalysts for excellent peroxymonosulfate activation towards antibiotics degradation. Chemical Engineering Journal 381, 122768

Xiu L, Wang Z, Yu M, Wu X, Qiu J (2018): Aggregation-resistant 3D MXene-based architecture as efficient bifunctional electrocatalyst for overall water splitting. ACS nano 12, 8017-8028

Yan J, Li J, Peng J, Zhang H, Zhang Y, Lai B (2019): Efficient degradation of sulfamethoxazole by the CuO@Al2O3 (EPC) coupled PMS system: Optimization, degradation pathways and toxicity evaluation. Chemical Engineering Journal 359, 1097-1110

Yang S, Wang P, Yang X, Shan L, Zhang W, Shao X, Niu R (2010): Degradation efficiencies of azo dye Acid Orange 7 by the interaction of heat, UV and anions with common oxidants: persulfate, peroxymonosulfate and hydrogen peroxide. Journal of hazardous materials 179, 552-558

Yu J, Zhang J, Zeng T, Wang H, Sun Y, Chen L, Song S, Shi H (2019): Stable incorporation of MnOx quantum dots into N-doped hollow carbon: a synergistic peroxymonosulfate activator for enhanced removal of bisphenol A. Separation and Purification Technology 213, 264-275

Zeng H, Deng L, Zhang H, Zhou C, Shi Z (2020): Development of oxygen vacancies enriched CoAl hydroxide@ hydroxysulfide hollow flowers for peroxymonosulfate activation: A highly efficient singlet oxygen-dominated oxidation process for sulfamethoxazole degradation. Journal of hazardous materials 400, 123297

Zeng H, Deng L, Yang L, Wu H, Zhang H, Zhou C, Liu B, Shi Z (2021): Novel Prussian blue analogues@ MXene nanocomposite as heterogeneous activator of peroxymonosulfate for the degradation of coumarin: The nonnegligible role of Lewis-acid sites on MXene. Chemical Engineering Journal 416, 128071

Zeng T, Yu M, Zhang H, He Z, Zhang X, Chen J, Song S (2017): In situ synthesis of cobalt ferrites-embedded hollow N-doped carbon as an outstanding catalyst for elimination of organic pollutants.

Science of the Total Environment 593, 286-296

Zhang H, Zhou C, Zeng H, Deng L, Shi Z (2020a): Can Cu2ZnSnS4 nanoparticles be used as heterogeneous catalysts for sulfadiazine degradation? Journal of hazardous materials 395, 122613

Zhang Q, He D, Li X, Feng W, Lyu C, Zhang Y (2020b): Mechanism and performance of singlet oxygen dominated peroxymonosulfate activation on CoOOH nanoparticles for 2,4-dichlorophenol degradation in water. Journal of Hazardous Materials 384, 121350

Zhang Q, He D, Li X, Feng W, Lyu C, Zhang Y (2020c): Mechanism and performance of singlet oxygen dominated peroxymonosulfate activation on CoOOH nanoparticles for 2, 4-dichlorophenol degradation in water. Journal of hazardous materials 384, 121350

Zhang Y, Guo B, Hu L, Xu Q, Li Y, Liu D, Xu M (2018): Synthesis of SnS nanoparticle-modified MXene (Ti3C2Tx) composites for enhanced sodium storage. Journal of Alloys and Compounds 732, 448-453

Zhao L, Dong B, Li S, Zhou L, Lai L, Wang Z, Zhao S, Han M, Gao K, Lu M (2017): Interdiffusion Reaction-Assisted Hybridization of Two-Dimensional Metal–Organic Frameworks and Ti3C2T x Nanosheets for Electrocatalytic Oxygen Evolution. ACS nano 11, 5800-5807

Zhou S, Yu Y, Zhang W, Meng X, Luo J, Deng L, Shi Z, Crittenden J (2018): Oxidation of microcystin-LR via activation of peroxymonosulfate using ascorbic acid: kinetic modeling and toxicity assessment. Environmental science & technology 52, 4305-4312

Zhu M, Miao J, Duan X, Guan D, Zhong Y, Wang S, Zhou W, Shao Z (2018): Postsynthesis growth of CoOOH nanostructure on SrCo0. 6Ti0. 4O3− δ perovskite surface for enhanced degradation of aqueous organic contaminants. ACS Sustainable Chemistry & Engineering 6, 15737-15748

Figures

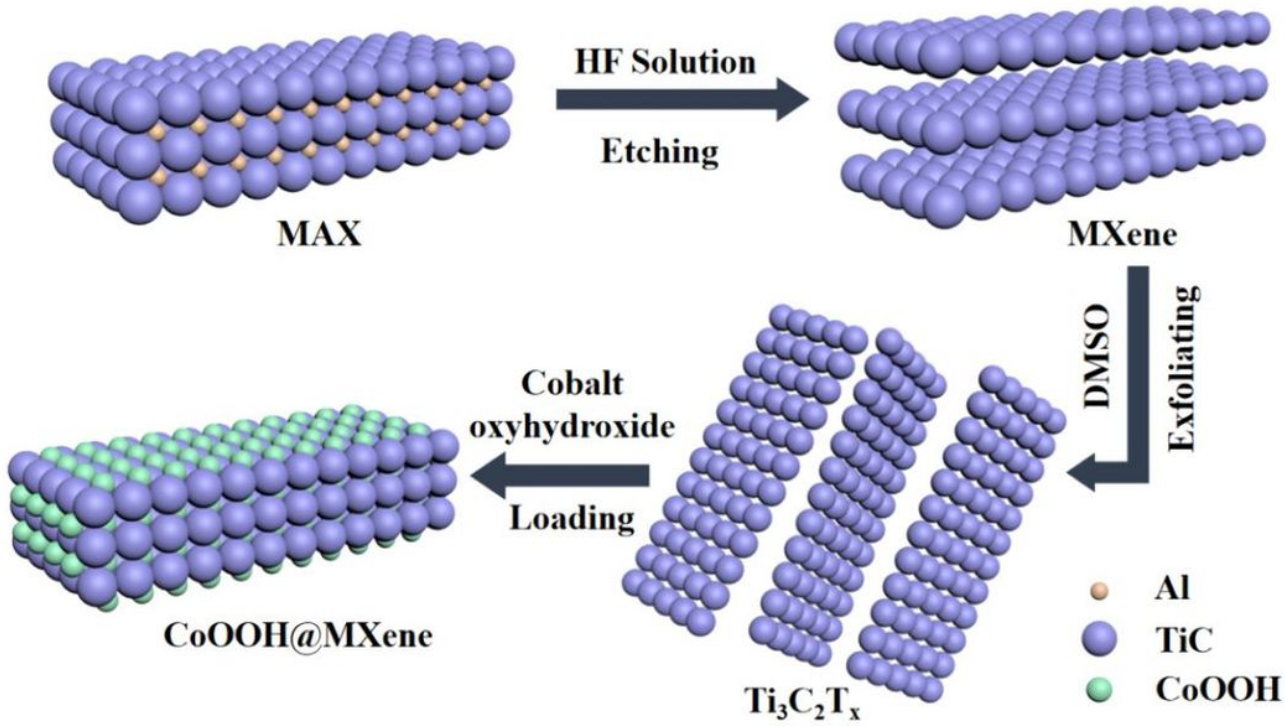

Figure 1

The synthesis route of CoOOH@MXene.

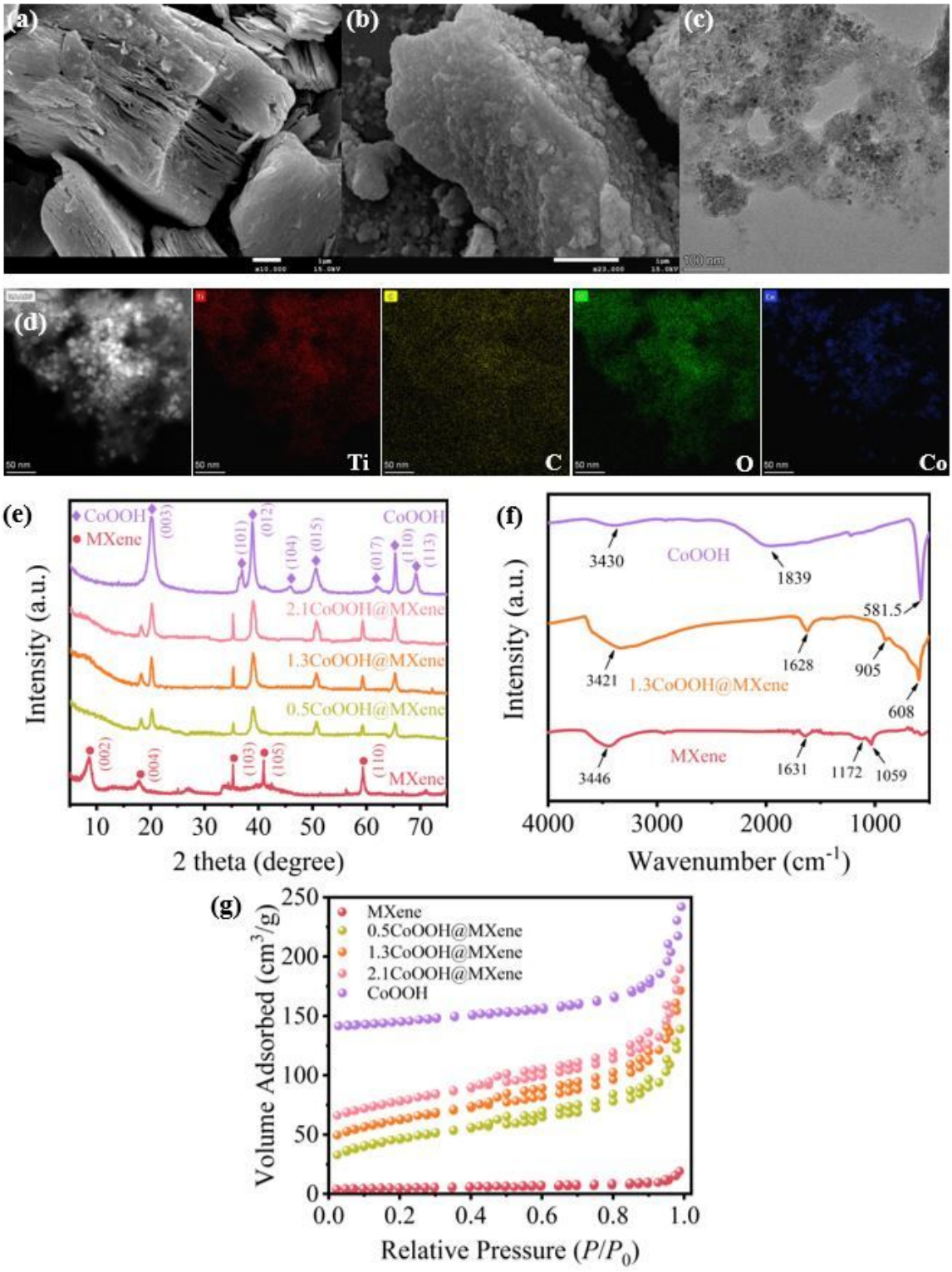

Figure 2

SEM images of (a) MXene and (b) 1.3CoOOH@MXene; (c) TEM image of 1.3CoOOH@MXene; (d) EDS elemental mapping images of 1.3CoOOH@MXene; (e) XRD pattern of CoOOH, MXene and various CoOOH@MXene; (f) FTIR spectra of CoOOH, MXene and 1.3CoOOH@MXene; (g) N_2 adsorption-desorption isotherms of CoOOH, MXene and various CoOOH@MXene.

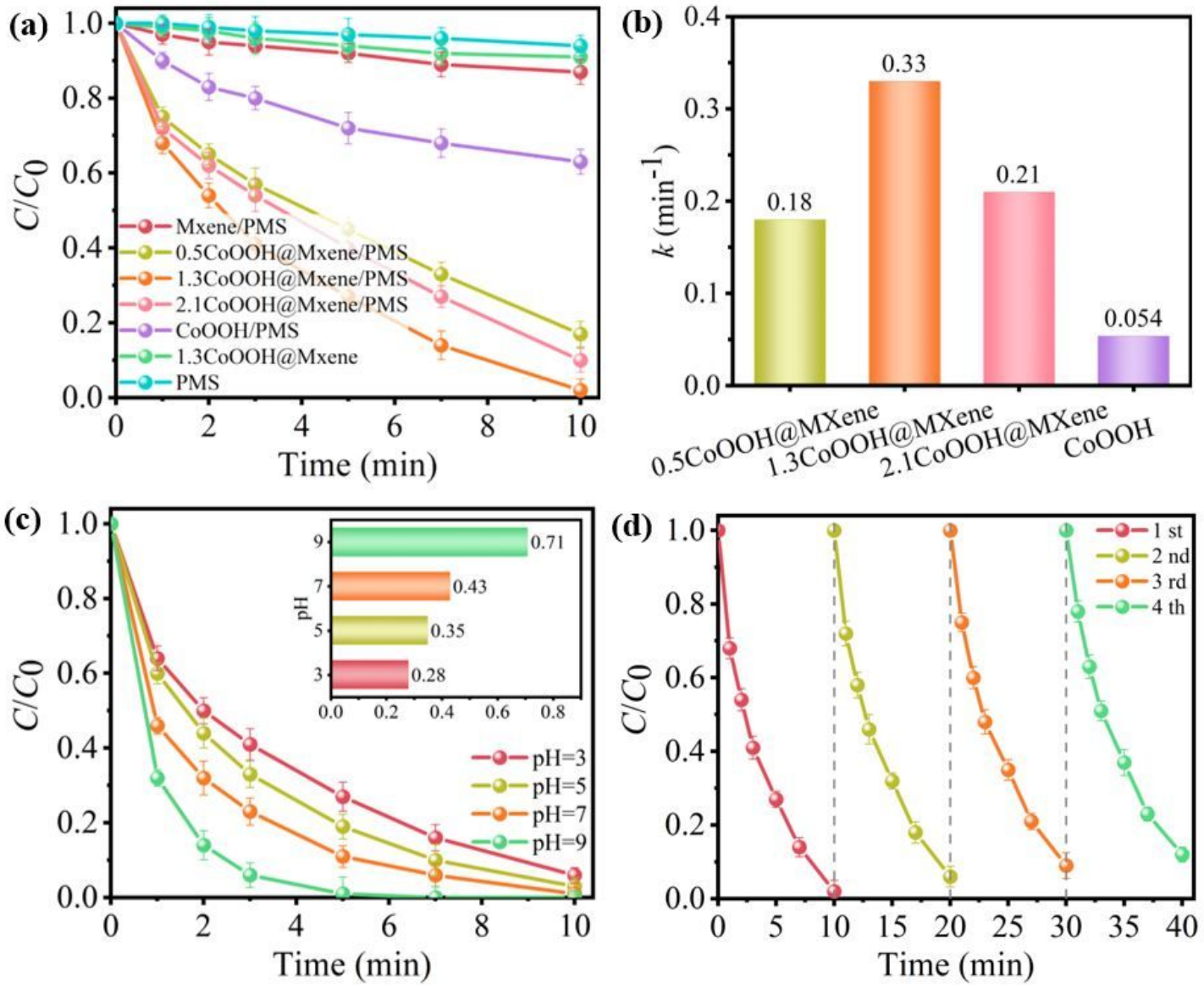

Figure 3

(a) The SMX degradation curves in different reaction systems ([PMS] = 0.5 mM, [catalyst] = 0.2 g/L, [SMX] = 20 μM, and without pH adjustment); (b) Corresponding *k* values determined by the pseudo-first-order kinetic model for CoOOH and various CoOOH@MXene; (c) Effect of initial solution pH on SMX degradation ([PMS] = 0.5 mM, [catalyst] = 0.2 g/L, [SMX] = 20 μM); (d) Reusability of 1.3CoOOH@MXene for SMX degradation ([PMS] = 0.5 mM, [catalyst] = 0.2 g/L, [SMX] = 20 μM, and without pH adjustment).

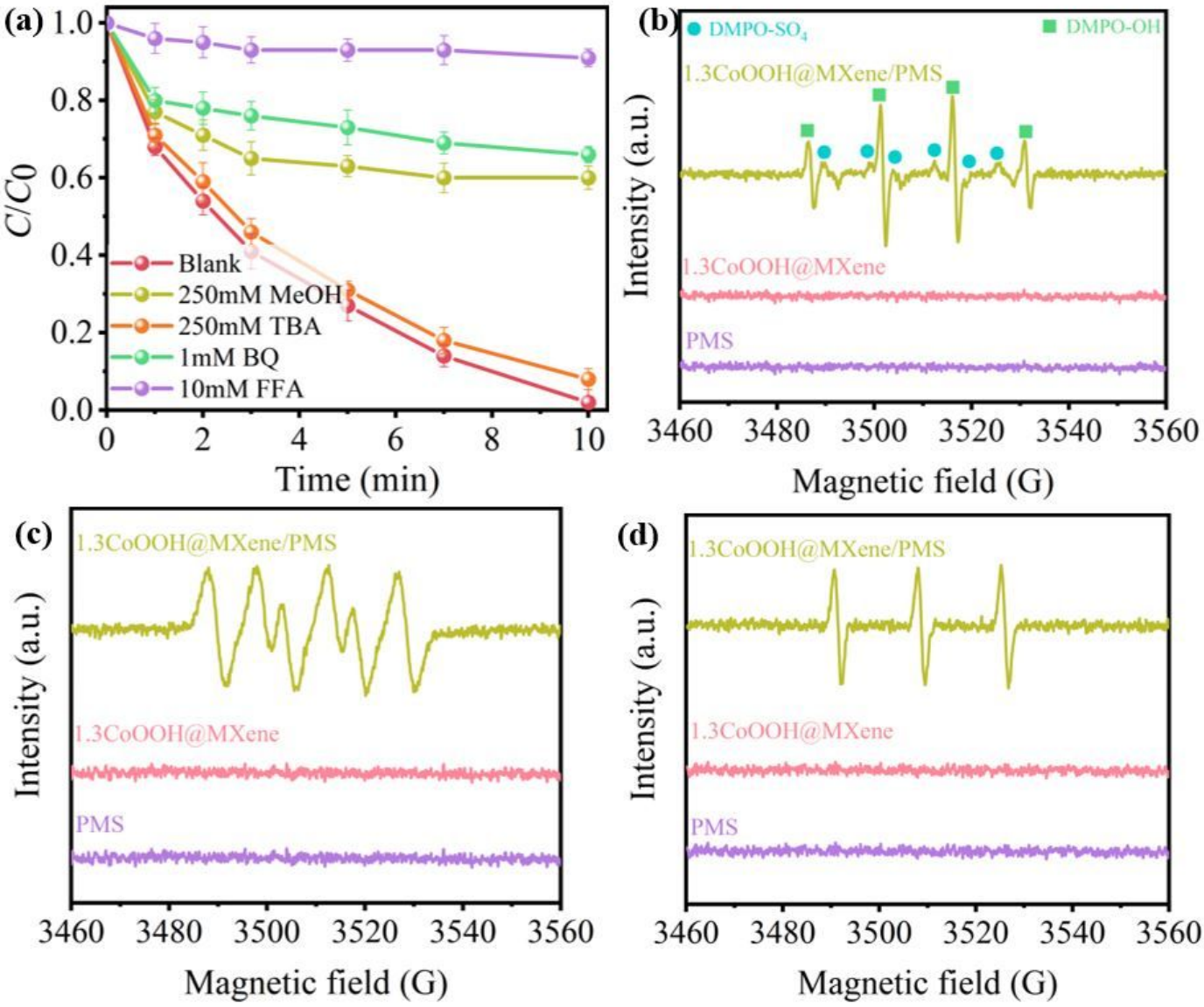

Figure 4

(a) Effect of different quenchers on SMX degradation; (b) EPR spectra of $SO_4^{\bullet-}$ and $^{\bullet}OH$; (c) EPR spectra of $O_2^{\bullet-}$; (d) EPR spectra of $^1O_2$ ([PMS] = 0.5 mM, [catalyst] = 0.1 g/L, [SMX] = 20 μM, [DMPO]=100 mM, [TEMP]=100 mM).

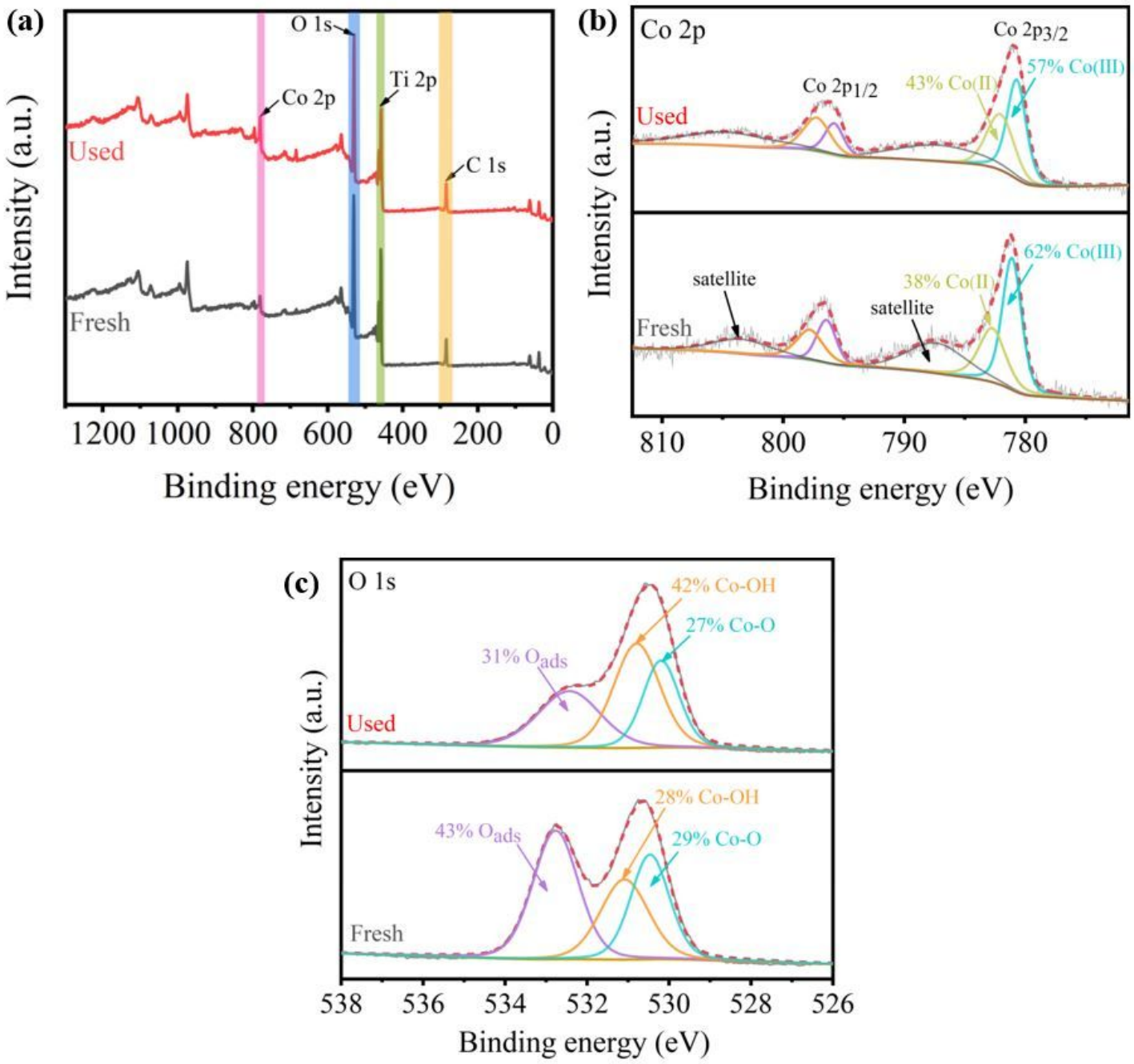

Figure 5

(a) The XPS spectra survey of fresh and used 1.3CoOOH@MXene; High-resolution XPS spectra of (b) Co 2p and (c) O 1s of fresh and used 1.3CoOOH@MXene.

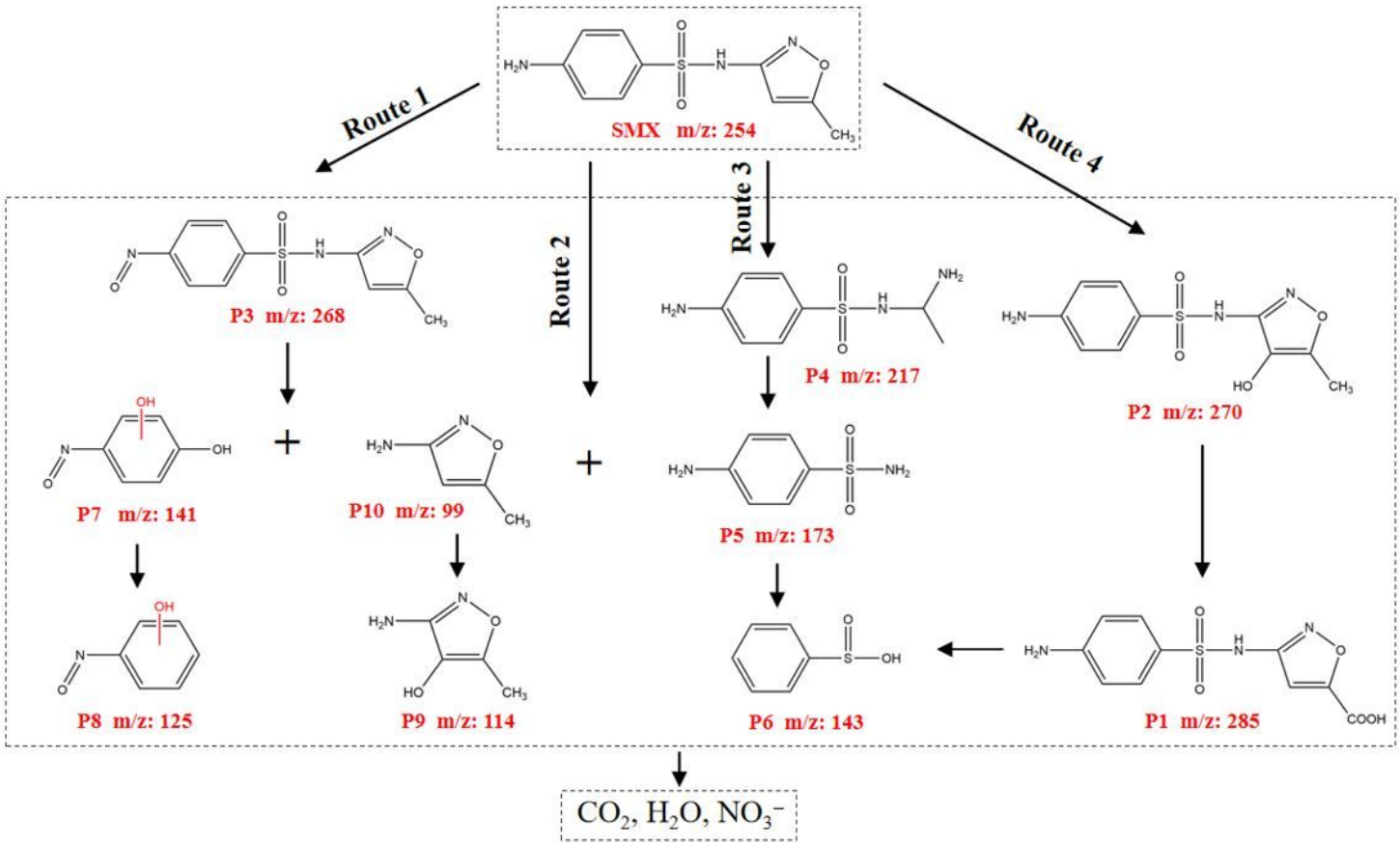

Figure 6

Possible degradation pathways of SMX in the 1.3CoOOH@MXene/PMS system.

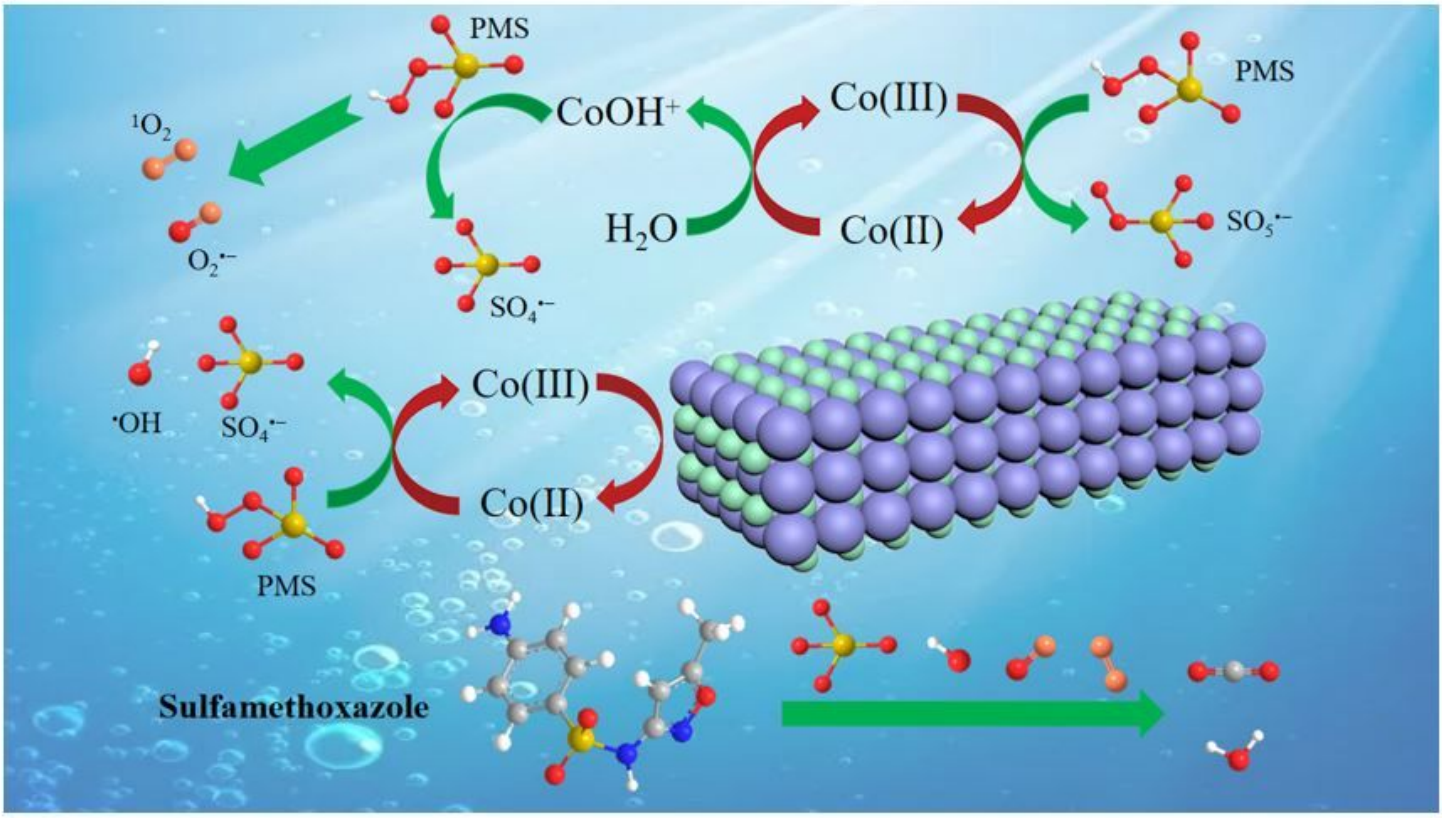

Figure 7

PMS activation mechanism by 1.3CoOOH@MXene for SMX degradation.

Supplementary Files

This is a list of supplementary files associated with this preprint. Click to download.

- SupplementaryMaterial.docx